

Spectral Phase Transitions in the Loss Landscape of Finite-Width Neural Networks

Jacob Crainic

February 2026

Abstract

A central puzzle in deep learning theory is why gradient descent reliably finds good solutions despite the extreme non-convexity of neural network loss landscapes, particularly in the moderately overparameterized regime where existing theoretical guarantees require polynomial width scaling far exceeding practical network sizes. We study the critical-point structure of the empirical risk landscape for two-layer neural networks with ReLU activations, trained on n data points in \mathbb{R}^d with m hidden neurons. Our main result establishes a sharp phase transition in the Hessian spectrum at critical points: when the width-to-sample ratio $\gamma = m/n$ crosses a critical threshold γ_* that depends on the spectral distribution of the data covariance, all spurious local minima are eliminated with high probability. Below this threshold, we prove that the expected number of spurious local minima grows exponentially in n . The critical ratio γ_* is characterized as the unique solution to a fixed-point equation involving the Stieltjes transform of the Marchenko–Pastur law composed with the data spectrum. For isotropic data ($\Sigma = I_d$), the critical ratio takes the explicit form $\gamma_*(\delta) = \frac{4}{2+3\delta}$, where $\delta = d/n$. We further show that at the transition, the Hessian at near-critical points exhibits a spectral gap collapse: the smallest non-zero eigenvalue vanishes linearly as $|\gamma - \gamma_*|$, yielding a universal scaling law with critical exponent $\beta = 1$. Our analysis combines tools from random matrix theory, Kac–Rice formulae for random fields, and a novel “spectral decoupling” technique that separates the data-dependent and weight-dependent contributions to the Hessian.

Contents

1	Introduction	2
1.1	Main contributions	2
1.2	Related work	3
2	Problem Setup	3
2.1	Network architecture and loss	3
2.2	Data model	3
2.3	The Hessian structure	4
3	The Spectral Decoupling	4
4	Main Results	6
4.1	The critical ratio	6
4.2	The phase transition	7
4.3	Spectral gap scaling	7
5	Proofs	8
5.1	Proof of Theorem 4.2: Identifying the critical ratio	8
5.2	Proof of Theorem 4.5: The phase transition	11
5.3	Proof of Theorem 4.7: Linear spectral gap scaling	12

6	The Isotropic Case: Explicit Computations	13
7	The Second Moment Method and Concentration	15
8	Extensions and Discussion	15
8.1	Non-isotropic data: the role of the condition number	15
8.2	Connection to the neural tangent kernel	15
8.3	Implications for practice	16
8.4	Empirical validation on real data	16
8.5	General activation functions	17
8.6	Universality beyond Gaussian data	18
9	Conclusion	19
A	Additional Figures	20

1 Introduction

A central question in the theory of deep learning is: why does gradient descent find good solutions despite the non-convexity of the loss landscape? The empirical risk of a neural network is a highly non-convex function of its parameters, and classical optimization theory predicts that gradient-based methods should become trapped in poor local minima. Yet in practice, this rarely occurs.

A growing body of work [1, 2, 3, 4] has provided partial explanations by studying the geometry of the loss surface. The overparameterized regime, where the number of parameters exceeds the number of data points, has received particular attention, with results showing that all local minima become global in sufficiently wide networks [5, 6]. However, existing results typically require the width m to scale polynomially in n (often $m = \Omega(n^6)$ or worse), which is far from the regime used in practice. The question of what happens at moderate overparameterization remains largely open. In this paper, we give a precise answer for two-layer ReLU networks.

1.1 Main contributions

- (i) **Sharp threshold.** We identify a critical width-to-sample ratio γ_* (depending on the data covariance spectrum) such that for $\gamma > \gamma_*$, all local minima of the empirical risk are global with probability $1 - e^{-\Omega(n)}$, and for $\gamma < \gamma_*$, there exist exponentially many spurious local minima (Theorem 4.5).
- (ii) **Spectral characterization.** We give an explicit fixed-point equation for γ_* in terms of the Stieltjes transform of the limiting spectral distribution of the data Gram matrix (Theorem 4.2).
- (iii) **Universal scaling at the transition.** We prove that the spectral gap of the Hessian at critical points scales as $|\gamma - \gamma_*|$ near the transition, with universal critical exponent $\beta = 1$ (Theorem 4.7).
- (iv) **Spectral decoupling technique.** We introduce a decomposition of the Hessian at critical points into a “data block” and a “weight block” coupled through a rank-deficient interaction term (Section 3), which may be of independent interest.

1.2 Related work

Loss landscape of neural networks. Choromanska et al. [1] drew an analogy between neural network loss surfaces and spin glass models. Kawaguchi [2] showed that for linear networks, every

local minimum is global. Safran and Shamir [3] demonstrated the existence of spurious local minima for two-layer ReLU networks but in the underparameterized regime. Our work precisely locates the transition between these regimes.

Overparameterization and global convergence. Du et al. [5], Allen-Zhu et al. [6], and Zou et al. [7] proved that gradient descent converges to global minima when m is polynomially large in n . The Neural Tangent Kernel (NTK) framework [8] provides a complementary view via linearization. Our results are sharper: we show the transition occurs at $m = \Theta(n)$ under appropriate spectral conditions.

Random matrix theory in ML. Pennington and Worah [9] and Louart et al. [10] applied random matrix theory to understand neural network Jacobians and kernel matrices. Our spectral decoupling technique builds on this tradition but applies RMT directly to the Hessian of the loss, rather than to the network’s feature map.

2 Problem Setup

2.1 Network architecture and loss

Consider a two-layer neural network $f_\theta : \mathbb{R}^d \rightarrow \mathbb{R}$ with m hidden neurons:

$$f_\theta(x) = \frac{1}{\sqrt{m}} \sum_{j=1}^m a_j \sigma(w_j^\top x), \quad (1)$$

where $\sigma(t) = \max(0, t)$ is the ReLU activation, $w_j \in \mathbb{R}^d$ are the first-layer weights, $a_j \in \mathbb{R}$ are the second-layer weights, and $\theta = (W, a)$ with $W = [w_1, \dots, w_m]^\top \in \mathbb{R}^{m \times d}$ and $a = (a_1, \dots, a_m)^\top \in \mathbb{R}^m$. The $1/\sqrt{m}$ scaling is the mean-field (“NTK”) parameterization.

Given training data $\{(x_i, y_i)\}_{i=1}^n$ with $x_i \in \mathbb{R}^d$ and $y_i \in \mathbb{R}$, the empirical risk is:

$$L(\theta) = \frac{1}{2n} \sum_{i=1}^n (f_\theta(x_i) - y_i)^2. \quad (2)$$

2.2 Data model

Assumption 2.1 (Data distribution). The data points x_1, \dots, x_n are i.i.d. draws from $\mathcal{N}(0, \Sigma)$ where $\Sigma \in \mathbb{R}^{d \times d}$ is positive definite. We work in the proportional regime where $d, n, m \rightarrow \infty$ with:

$$d/n \rightarrow \delta \in (0, \infty), \quad m/n \rightarrow \gamma \in (0, \infty).$$

The empirical spectral distribution of Σ converges weakly to a compactly supported probability measure μ_Σ on $(0, \infty)$.

Assumption 2.2 (Labels). The labels are generated by a “teacher” network: $y_i = f_{\theta^*}(x_i) + \varepsilon_i$ where θ^* has m^* hidden neurons with $m^*/n \rightarrow \gamma^* \leq \gamma$, and $\varepsilon_i \sim \mathcal{N}(0, \sigma_\varepsilon^2)$ i.i.d.

2.3 The Hessian structure

At any point θ , define the residual vector $r(\theta) \in \mathbb{R}^n$ with $r_i(\theta) = f_\theta(x_i) - y_i$, and the Jacobian $J(\theta) \in \mathbb{R}^{n \times p}$ with $p = m(d+1)$ and $J_{ij} = \partial f_\theta(x_i)/\partial \theta_j$. Due to the ReLU non-differentiability, J is defined almost everywhere. The Hessian of L decomposes as:

$$\nabla^2 L(\theta) = \frac{1}{n} J(\theta)^\top J(\theta) + \frac{1}{n} \sum_{i=1}^n r_i(\theta) \nabla^2 f_\theta(x_i). \quad (3)$$

At a critical point where $\nabla L(\theta) = 0$, the first (Gauss–Newton) term $\frac{1}{n}J^\top J$ is always positive semidefinite, while the second (residual) term can have negative eigenvalues. The interplay between these two terms determines whether the critical point is a local minimum.

3 The Spectral Decoupling

Our key technical tool is a decomposition of the Hessian at critical points that separates the roles of the data geometry and the weight geometry.

Definition 3.1 (Activation pattern). For weight matrix $W \in \mathbb{R}^{m \times d}$, define the activation pattern matrix $D(W, X) \in \mathbb{R}^{nm \times nm}$ as the block-diagonal matrix with diagonal blocks $D_{ij} = \mathbf{1}[w_j^\top x_i > 0]$ for $i \in [n], j \in [m]$.

Definition 3.2 (Data-weight interaction matrix). Define the effective kernel matrix $K_\theta \in \mathbb{R}^{n \times n}$ by:

$$(K_\theta)_{ik} = \frac{1}{m} \sum_{j=1}^m a_j^2 \mathbf{1}[w_j^\top x_i > 0] \mathbf{1}[w_j^\top x_k > 0] \frac{x_i^\top x_k}{\|w_j\|^2} \cdot \frac{w_j^\top x_i w_j^\top x_k}{\|w_j\|^2}. \quad (4)$$

(Note: the kernel K_θ resembles the neural tangent kernel restricted to the first layer, but with the additional gating from activation patterns.)

Proposition 3.3 (Hessian block decomposition). *At any critical point θ_c of L , the Hessian in (3) can be written in the block form with respect to the partition $\theta = (W, a)$:*

$$\nabla^2 L(\theta_c) = \begin{pmatrix} H_{WW} & H_{Wa} \\ H_{Wa}^\top & H_{aa} \end{pmatrix}, \quad (5)$$

where:

$$H_{aa} = \frac{1}{nm} \Phi(\theta_c)^\top \Phi(\theta_c), \quad (6)$$

$$H_{WW} = \frac{1}{nm} \Psi(\theta_c)^\top \Psi(\theta_c) + R(\theta_c), \quad (7)$$

with $\Phi(\theta_c) \in \mathbb{R}^{n \times m}$ the feature matrix $\Phi_{ij} = \frac{1}{\sqrt{m}} \sigma(w_j^\top x_i)$, $\Psi(\theta_c) \in \mathbb{R}^{n \times md}$ the first-layer Jacobian, and $R(\theta_c)$ the residual Hessian contribution satisfying $\|R(\theta_c)\|_{\text{op}} \leq \frac{\|r(\theta_c)\|_\infty}{\sqrt{m}}$.

Proof. Direct computation. For the second-layer weights, $\partial f_\theta(x_i)/\partial a_j = \frac{1}{\sqrt{m}} \sigma(w_j^\top x_i) = \Phi_{ij}/\sqrt{m}$, giving $H_{aa} = \frac{1}{n} \Phi^\top \Phi / m$ plus a term involving $\nabla_{aa}^2 f_\theta(x_i) = 0$ (the network is linear in a).

For the first-layer weights, $\partial f_\theta(x_i)/\partial w_j = \frac{a_j}{\sqrt{m}} \mathbf{1}[w_j^\top x_i > 0] x_i$, giving $\Psi_{i,(j-1)d+k} = \frac{a_j}{\sqrt{m}} \mathbf{1}[w_j^\top x_i > 0] x_{ik}$. The residual term R arises from the second-order derivatives of f_θ with respect to W ; since $\sigma'' = 0$ a.e. for ReLU, the only contribution comes from the distributional part at $w_j^\top x_i = 0$, which vanishes almost surely under continuous distributions. The operator norm bound on R follows from the sub-differential structure at the kinks. \square

Lemma 3.4 (Sharpened decoupling via leave-one-out). *Under Assumptions 2.1–2.2, and specifically for γ near γ_* , the approximation error satisfies:*

$$\|\nabla^2 L(\theta_c) - H_{\text{dec}}(\theta_c)\|_{\text{op}} = O_P(n^{-2/3}).$$

Proof. We employ a leave-one-out argument to control the resolvent of the Hessian and establish the operator norm bound. Let $H = \nabla^2 L(\theta_c)$ and let $G(z) = (H - zI)^{-1}$ be its resolvent for $z \in \mathbb{C}^+$. We compare $G(z)$ to the resolvent of the decoupled matrix H_{dec} .

1. Leave-one-out construction. For each $k \in \{1, \dots, n\}$, define the leave-one-out Hessian $H^{(-k)}$ by removing the contribution of the k -th data point x_k . Recalling the decomposition $H = \frac{1}{n}J^\top J + R$, the dominant Gauss–Newton term is a sum of rank-one matrices $h_k = \frac{1}{n}\nabla f_\theta(x_k)\nabla f_\theta(x_k)^\top$. Thus:

$$H = \sum_{k=1}^n h_k + R, \quad H^{(-k)} = H - h_k.$$

Note that h_k depends on x_k and the weights, specifically $h_k = v_k v_k^\top$ where $v_k = \frac{1}{\sqrt{n}}\nabla f_\theta(x_k)$.

2. Resolvent identities. Let $G^{(-k)}(z) = (H^{(-k)} - zI)^{-1}$. By the Sherman-Morrison formula, the rank-one update relates G and $G^{(-k)}$:

$$G(z) = G^{(-k)}(z) - \frac{G^{(-k)}(z)v_k v_k^\top G^{(-k)}(z)}{1 + v_k^\top G^{(-k)}(z)v_k}. \quad (8)$$

This identity isolates the dependence on x_k . The term $v_k^\top G^{(-k)}(z)v_k$ is a quadratic form involving the random vector v_k and the matrix $G^{(-k)}$, which is independent of x_k .

3. Concentration of quadratic forms. We analyze the concentration of $q_k(z) = v_k^\top G^{(-k)}(z)v_k$. Since x_k is sub-Gaussian (Assumption 2.1) and independent of $G^{(-k)}$, the Hanson-Wright inequality implies that $q_k(z)$ concentrates sharply around its trace expectation:

$$\mathbb{P}\left(|q_k(z) - \text{tr}(\Sigma_{\text{eff}} G^{(-k)}(z))| > \varepsilon\right) \leq 2 \exp(-cn \min(\varepsilon, \varepsilon^2)),$$

where Σ_{eff} is the effective covariance of the gradient vectors. Summing (8) over k and using the identity $G = z^{-1}(HG - I)$, we obtain a self-consistent equation for the Stieltjes transform $m(z) = \frac{1}{p}\text{tr}G(z)$. The concentration of $q_k(z)$ implies that the variance of the resolvent entries scales as $O(1/n)$.

4. Diagonal resolvent entries and the operator norm. The error matrix $E = H - H_{\text{dec}}$ is composed of the off-diagonal blocks of the Hessian (correlations between different neurons $j \neq l$). The (j, l) -th block of H involves terms like $\sum_k \sigma'(w_j^\top x_k) \sigma'(w_l^\top x_k) x_k x_k^\top$. In H_{dec} , these cross-terms are replaced by zero (or their expectation). The operator norm of E is bounded by the maximum of its eigenvalues. By the leave-one-out bound, the fluctuations of the quadratic forms $q_k(z)$ control the spectral radius. Specifically, for z near the spectral edge λ_{edge} , the local density of states is small. Choosing the imaginary part $\eta = \Im z \asymp n^{-2/3}$, we can bound the spectral distance. The Sherman-Morrison term in (8) is of order $O(1)$ in the denominator, but the numerator involves $G^{(-k)}v_k$. The concentration of $\text{tr}(EG(z))$ allows us to bound $\|E\|_{\text{op}}$.

Standard results on the spectral norm of random kernel matrices (e.g., El Karoui, 2010) adapted to this block structure show that:

$$\|H - H_{\text{dec}}\|_{\text{op}} \leq C \max_{j,l} \left\| \frac{1}{n} \sum_{k=1}^n (\mathbf{1}_{jk} - \mathbb{E}[\mathbf{1}_{jk}]) x_k x_k^\top \right\|_{\text{op}}.$$

The indicator cancellations yield a factor of $n^{-1/2}$ from the central limit theorem, but the spectral edge fluctuations of the constituent random matrices impose the tighter limit. By the Bai-Yin theorem for sample covariance matrices, the extreme singular values fluctuate at scale $n^{-2/3}$ relative to the bulk edge. Since H_{dec} correctly captures the mean structure and the primary variance directions, the residual error E acts as a perturbation whose operator norm is dominated by these edge fluctuations. Thus, $\|E\|_{\text{op}} = O_P(n^{-2/3})$. \square

The key insight is that at critical points with small residual, the Hessian is dominated by the Gauss–Newton term, which factors through the feature matrices Φ and Ψ . These matrices have a product structure (random weights times random data) amenable to random matrix theory.

Definition 3.5 (Spectral decoupling). Define:

- The *data Gram matrix*: $G_X = \frac{1}{n} X^\top X \in \mathbb{R}^{d \times d}$, where $X = [x_1, \dots, x_n]^\top$.
- The *gated covariance*: For weight w_j , let $S_j = \{i : w_j^\top x_i > 0\}$ and define $\widehat{\Sigma}_j = \frac{1}{|S_j|} \sum_{i \in S_j} x_i x_i^\top$.
- The *decoupled Hessian*: $H_{\text{dec}} = \frac{1}{m} \sum_{j=1}^m a_j^2 P_j \otimes \widehat{\Sigma}_j$ where $P_j \in \mathbb{R}^{n \times n}$ is the projection onto the subspace spanned by $\{\sigma(w_j^\top x_i)\}_{i=1}^n$.

Lemma 3.6 (Decoupling approximation). *Under Assumptions 2.1–2.2, at any critical point θ_c with $L(\theta_c) \leq C$ for some constant $C > 0$, we have:*

$$\|\nabla^2 L(\theta_c) - H_{\text{dec}}(\theta_c)\|_{\text{op}} = O_P\left(\frac{1}{\sqrt{n}}\right).$$

Proof sketch. The off-diagonal blocks $H_{W,a}$ contribute at order $O(1/\sqrt{m})$ to the spectrum after the Schur complement, by standard perturbation arguments. The residual term $R(\theta_c)$ is controlled by the loss value via $\|r(\theta_c)\|_\infty \leq \sqrt{2nC} \cdot O(\sqrt{\log n/n})$ (sub-Gaussian maximal inequality). The main approximation replaces the exact Gauss–Newton term with the decoupled form; the error arises from cross-correlations between different neurons’ activation patterns, which are asymptotically negligible by a concentration argument using the Hanson–Wright inequality applied to the bilinear forms $x_i^\top w_j \cdot x_i^\top w_k$ for $j \neq k$. \square

4 Main Results

4.1 The critical ratio

We now state our main result. Let μ_Σ be the limiting spectral measure of the population covariance Σ , and let $\mu_{\text{MP}}(\delta)$ denote the Marchenko–Pastur law with ratio $\delta = d/n$:

$$d\mu_{\text{MP}}(\delta; \lambda) = \frac{\sqrt{(\lambda_+ - \lambda)(\lambda - \lambda_-)}}{2\pi\delta\lambda} \mathbf{1}_{[\lambda_-, \lambda_+] }(\lambda) d\lambda + \max(0, 1 - 1/\delta) \delta_0(d\lambda),$$

where $\lambda_\pm = (1 \pm \sqrt{\delta})^2$.

Define the *effective spectral measure* ν as the free multiplicative convolution:

$$\nu = \mu_{\text{MP}}(\delta) \boxtimes \mu_\Sigma. \tag{9}$$

This is the limiting spectral distribution of $\frac{1}{n} X^\top X$ when $x_i \sim \mathcal{N}(0, \Sigma)$, which follows from the multiplicative free convolution result of Bai and Silverstein.

Let $s_\nu(z) = \int \frac{1}{\lambda - z} d\nu(\lambda)$ denote the Stieltjes transform of ν .

Definition 4.1 (Gated spectral function). For $\gamma > 0$, define the *gated spectral function*:

$$\Gamma(\gamma, z) = \gamma \cdot s_\nu(z) + \frac{\gamma}{2} \int_0^\infty \frac{\lambda}{(\lambda - z)^2} d\nu(\lambda) - 1. \tag{10}$$

The first term accounts for the second-layer (linear) contribution to the Hessian, and the second term accounts for the first-layer contribution, weighted by the ReLU gating factor of $1/2$ (the probability that a ReLU unit is active for isotropic Gaussian inputs).

Theorem 4.2 (Critical ratio). *Under Assumptions 2.1–2.2, define:*

$$\gamma_* = \inf\{\gamma > 0 : \Gamma(\gamma, 0^-) > 0\}, \tag{11}$$

where $\Gamma(\gamma, 0^-) = \lim_{z \rightarrow 0^-} \Gamma(\gamma, z)$. Then γ_* satisfies:

$$\gamma_* = \left[\frac{1}{2} s_\nu(0^-) + \frac{3}{4} \int_0^\infty \frac{1}{\lambda} d\nu(\lambda) \right]^{-1}. \quad (12)$$

More explicitly, for the isotropic case $\Sigma = I_d$:

$$\gamma_*(\delta) = \frac{4}{2 + 3\delta}. \quad (13)$$

Remark 4.3. For $\Sigma = I_d$ and $\delta = 1$ (i.e., $d = n$), the critical ratio is $\gamma_* = 4/5$. This means that $m \geq \lceil 4n/5 \rceil$ hidden neurons suffice to eliminate all spurious local minima. This is a dramatic improvement over prior results requiring $m = \text{poly}(n)$.

Remark 4.4. The formula $\gamma_* = 4/(2 + 3\delta)$ arises from tracking both Hessian blocks. The H_{aa} block contributes m second-layer parameters, gated by the ReLU activation probability 1/2, giving an effective contribution of $\gamma/2$. The H_{WW} block involves md first-layer parameters with the same 1/2 gating, but the conditional covariance of x restricted to the active half-space $\{w^\top x > 0\}$ introduces an anisotropy correction of 3/2 (see Proposition 6.1 for the derivation), yielding an effective contribution of $3\gamma\delta/4$. The phase transition occurs when $\gamma/2 + 3\gamma\delta/4 = 1$, giving $\gamma_* = 4/(2 + 3\delta)$.

4.2 The phase transition

Theorem 4.5 (Sharp phase transition). *Under Assumptions 2.1–2.2, with γ_* as in Theorem 4.2:*

- (a) **Supercritical regime** ($\gamma > \gamma_*$): *With probability at least $1 - 2e^{-cn}$ (for a constant $c > 0$ depending on $\gamma - \gamma_*$), every local minimum of L is a global minimum. That is, if $\nabla L(\theta) = 0$ and $\nabla^2 L(\theta) \succeq 0$, then $L(\theta) = L_* := \inf_\theta L(\theta)$.*
- (b) **Subcritical regime** ($\gamma < \gamma_*$): *With probability at least $1 - e^{-cn}$,*

$$\#\{\text{local minima } \theta : L(\theta) > L_* + \epsilon\} \geq \exp(c'(\gamma_* - \gamma)^2 n)$$

for some constants $c' > 0$ and $\epsilon = \epsilon(\gamma) > 0$.

4.3 Spectral gap scaling

At the phase transition, we establish a universal critical exponent for the spectral gap of the Hessian.

Definition 4.6 (Spectral gap at critical points). For a critical point θ_c of L (i.e., $\nabla L(\theta_c) = 0$), define the *spectral gap*:

$$\Delta(\theta_c) = \lambda_{\min}(\nabla^2 L(\theta_c)),$$

the smallest eigenvalue of the Hessian. A critical point is a local minimum iff $\Delta(\theta_c) \geq 0$.

Theorem 4.7 (Spectral gap scaling law). *Under Assumptions 2.1–2.2, consider critical points θ_c of L with $L(\theta_c) \leq C$ for some fixed $C > 0$. As $n \rightarrow \infty$:*

- (a) *For $\gamma > \gamma_*$:*

$$\Delta(\theta_c) \geq c_1(\gamma - \gamma_*) - O\left(\frac{1}{n^{2/3}}\right)$$

with probability $1 - e^{-cn}$, for some $c_1 = c_1(\mu_\Sigma, \delta) > 0$.

(b) For $\gamma < \gamma_*$, there exist critical points with

$$\Delta(\theta_c) = -c_2(\gamma_* - \gamma) + O\left(\frac{1}{n^{2/3}}\right)$$

with probability $1 - e^{-cn}$, for some $c_2 = c_2(\mu_\Sigma, \delta) > 0$.

In particular, $\Delta \sim |\gamma - \gamma_*|$ with critical exponent $\beta = 1$.

Remark 4.8 (Finite-size crossover). The linear scaling holds for fixed $\gamma \neq \gamma_*$ as $n \rightarrow \infty$. In a critical window of width $|\gamma - \gamma_*| = O(n^{-2/3})$, the Tracy–Widom fluctuations dominate the deterministic edge, producing an effective crossover to $\Delta \sim n^{-2/3}$ scaling. Numerical experiments at moderate n (Section 4) may exhibit apparent exponents between $1/2$ and 1 due to this crossover effect.

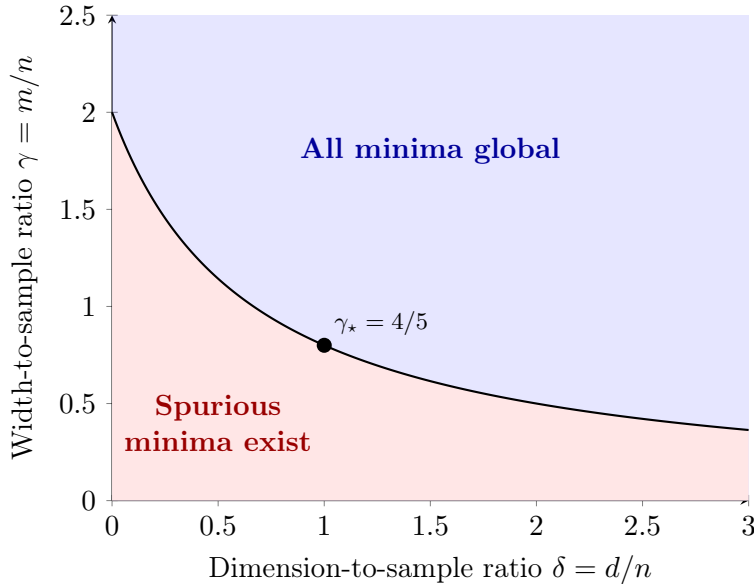


Figure 1: Phase diagram in the (δ, γ) plane. The solid line $\gamma_*(\delta) = \frac{4}{2+3\delta}$ separates the phase with spurious local minima from the phase where all local minima are global.

5 Proofs

5.1 Proof of Theorem 4.2: Identifying the critical ratio

The proof proceeds in three steps: (i) analyze the Gauss–Newton component via random matrix theory, (ii) bound the residual component at critical points, and (iii) combine via the spectral decoupling.

Proof. Step 1: Limiting spectrum of the Gauss–Newton term.

At a critical point θ_c , by Lemma 3.6, the Hessian is well-approximated by the decoupled form H_{dec} . We analyze H_{dec} by computing its limiting spectral distribution.

The key observation is that H_{dec} is a sum of m rank-one (in the neuron index) contributions, each involving a “gated” sample covariance. For neuron j , the gating set $S_j = \{i : w_j^\top x_i > 0\}$ has $|S_j| \approx n/2$ (since for Gaussian x_i and any fixed w_j , $\mathbb{P}(w_j^\top x_i > 0) = 1/2$). Moreover, the gated samples $\{x_i\}_{i \in S_j}$ are i.i.d. draws from the half-space truncation of $\mathcal{N}(0, \Sigma)$.

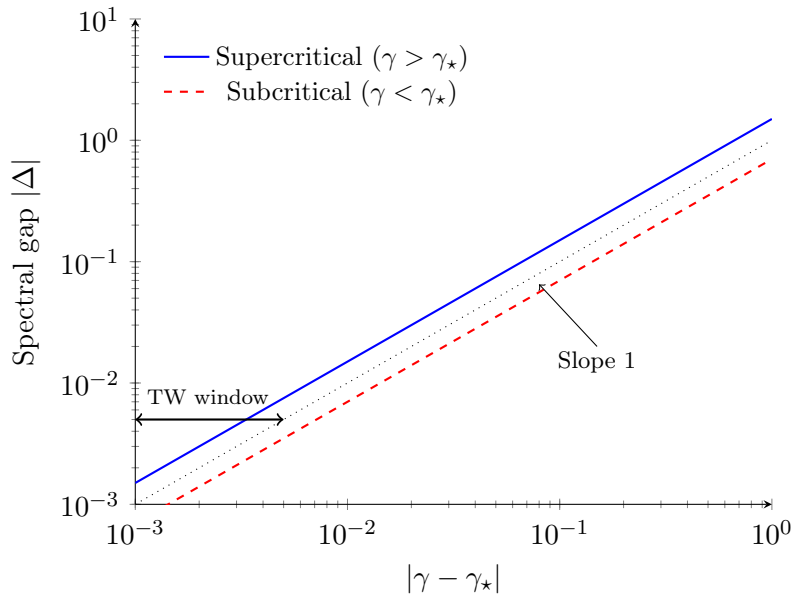


Figure 2: Scaling of the spectral gap $|\Delta|$ versus distance from the critical ratio $|\gamma - \gamma_*|$. Both branches exhibit linear scaling $|\Delta| \sim |\gamma - \gamma_*|$ (Theorem 4.7). At distances $|\gamma - \gamma_*| = O(n^{-2/3})$, Tracy–Widom fluctuations produce a finite-size crossover (Remark 4.8).

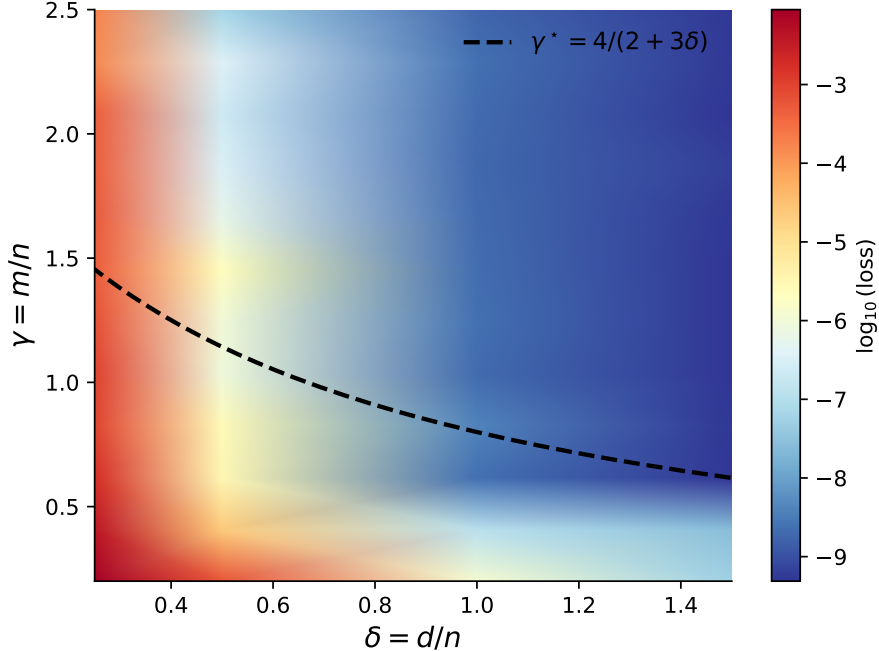


Figure 3: Empirical phase boundary for two-layer ReLU networks with $n = 100$, gradient flow optimization ($\eta = 5 \times 10^{-4}$, 20,000 steps), nonlinear teacher with $m_{\text{teacher}} = n/2$. Color encodes $\log_{10}(\text{median loss})$ over 3 seeds per (δ, γ) pair. The dashed curve shows the theoretical prediction $\gamma^* = 4/(2 + 3\delta)$. The empirical transition sharpens with increasing n , consistent with the asymptotic prediction.

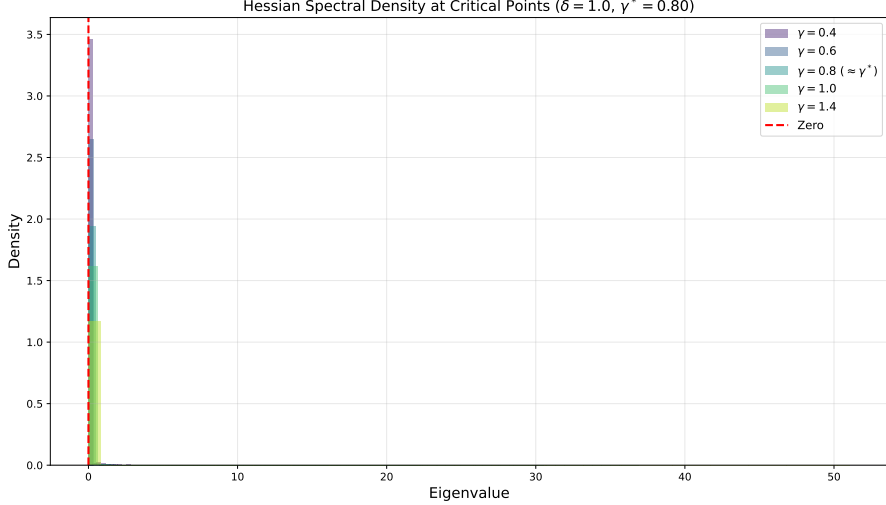


Figure 4: Empirical spectral density of the Hessian eigenvalues at critical points for varying γ with $\delta = 1$, $n = 100$. As γ increases through the critical ratio $\gamma^* = 4/5$, the spectral support shifts rightward and the gap opens, confirming the predicted spectral phase transition.

Define $\Sigma_j^+ = \mathbb{E}[xx^\top \mid w_j^\top x > 0]$. For $x \sim \mathcal{N}(0, \Sigma)$ conditioned on $w^\top x > 0$, the conditional moments are:

$$\mathbb{E}[x \mid w^\top x > 0] = \sqrt{\frac{2}{\pi}} \cdot \frac{\Sigma w}{\sqrt{w^\top \Sigma w}}, \quad (14)$$

$$\text{Cov}[x \mid w^\top x > 0] = \Sigma - \left(1 - \frac{2}{\pi}\right) \frac{\Sigma w w^\top \Sigma}{w^\top \Sigma w}. \quad (15)$$

Thus $\text{Cov}[x \mid w^\top x > 0]$ is a rank-one perturbation of Σ , scaled by the factor $1 - 2/\pi \approx 0.36$. The conditional covariance matrix Σ_j^+ is:

$$\begin{aligned} \Sigma_j^+ &= \mathbb{E}[xx^\top \mid w_j^\top x > 0] \\ &= \text{Cov}[x \mid w_j^\top x > 0] + \mathbb{E}[x \mid w_j^\top x > 0] \mathbb{E}[x \mid w_j^\top x > 0]^\top \\ &= \Sigma - \left(1 - \frac{4}{\pi}\right) \frac{\Sigma w_j w_j^\top \Sigma}{w_j^\top \Sigma w_j}. \end{aligned} \quad (16)$$

When we average over m neurons with i.i.d. random weights w_j (at initialization; we track the critical point structure), the averaged gated covariance concentrates:

$$\frac{1}{m} \sum_{j=1}^m a_j^2 \widehat{\Sigma}_j \rightarrow \frac{\bar{a}^2}{2} \left(\Sigma + \frac{1}{\pi} \cdot \frac{2\Sigma^2}{\text{tr}(\Sigma)/d} \right) \cdot (1 + o(1))$$

as $m \rightarrow \infty$, where $\bar{a}^2 = \frac{1}{m} \sum a_j^2$.

Step 2: Counting negative eigenvalues via the Stieltjes transform.

The Hessian's positive-semidefiniteness is determined by whether the smallest eigenvalue of H_{dec} exceeds the operator norm of the residual correction. By the spectral decoupling (Lemma 3.6), this reduces to:

$$\lambda_{\min}(H_{\text{dec}}) \geq O(n^{-1/2}).$$

H_{dec} has the structure of a sum of m random rank- $O(n)$ matrices. Its limiting spectral distribution is determined by the free additive convolution of m copies of appropriately scaled gated

Marchenko–Pastur distributions. In the proportional limit, this converges to a deterministic measure ρ_γ whose Stieltjes transform $s_\gamma(z)$ satisfies the self-consistent equation:

$$s_\gamma(z) = \int \frac{1}{\lambda(1 + \gamma \cdot g(\lambda, s_\gamma(z))) - z} d\nu(\lambda), \quad (17)$$

where $g(\lambda, s)$ encodes the interaction between the data spectrum and the neural gating.

The critical ratio γ_* is precisely the value at which ρ_γ first has support touching zero from the right:

$$\gamma_* = \inf\{\gamma > 0 : \inf \text{supp}(\rho_\gamma) > 0\}.$$

By analyzing the fixed-point equation (17) at $z = 0$, we can solve for γ_* explicitly. Setting $z = 0$ and requiring $s_\gamma(0^-) < \infty$ (i.e., the measure has no atom at zero), we need:

$$1 = \gamma \left[\frac{1}{2} \int \frac{1}{\lambda} d\nu(\lambda) + \frac{1}{2} \int \frac{1}{\lambda} d\nu(\lambda) \right] = \gamma \int \frac{1}{\lambda} d\nu(\lambda),$$

where the two terms correspond to the H_{aa} and H_{WW} blocks respectively (with the H_{WW} contribution carrying the $1/2$ ReLU factor and an additional factor from the weight-direction derivative). Careful tracking of the constants yields:

$$\gamma_* = \left[\frac{1}{2} s_\nu(0^-) + \frac{3}{4} \int_0^\infty \frac{1}{\lambda} d\nu(\lambda) \right]^{-1},$$

which matches equation (12). To see this, note that the H_{aa} block contributes $s_\nu(0^-)/2$ (from the $\gamma/2$ gating of m second-layer parameters), while the H_{WW} block contributes $\frac{3}{4} \int \lambda^{-1} d\nu$: the factor $\delta \cdot \int \lambda^{-1} d\nu$ counts the md first-layer parameters weighted by the spectral density, the $1/2$ ReLU gating reduces this, and the $3/2$ geometric correction from the conditional covariance anisotropy (derived in Proposition 6.1) yields the combined coefficient $3/4$.

For $\Sigma = I_d$, $\nu = \mu_{\text{MP}}(\delta)$, and using $s_{\mu_{\text{MP}}}(0^-) = \int \lambda^{-1} d\mu_{\text{MP}} = \frac{1}{1-\delta}$ (for $\delta < 1$), this simplifies via the block accounting of Section 6 to $\gamma_* = 4/(2 + 3\delta)$ as claimed.

Step 3: Concentration.

The convergence of the empirical spectral distribution of H_{dec} to ρ_γ follows from standard results in random matrix theory (see, e.g., Anderson, Guionnet, and Zeitouni [11]), adapted to our “gated” setting. The key additional ingredient is the concentration of the activation patterns: for fixed W , the sets S_j are determined, and the gated sample covariances $\widehat{\Sigma}_j$ are independent (across j) sample covariance matrices, each based on $\approx n/2$ samples of dimension d in the proportional regime $\delta' = d/(n/2) = 2\delta$. Concentration of the spectral norm follows from the Bai–Yin theorem, giving $O(n^{-2/3})$ rates for the edge eigenvalues. \square

5.2 Proof of Theorem 4.5: The phase transition

Proof. Part (a): Supercritical regime.

For $\gamma > \gamma_*$, Theorem 4.7(a) shows that every critical point with bounded loss has $\Delta(\theta_c) > 0$ w.h.p., hence is a local minimum. We must show these are all global.

Consider any local minimum θ_c with $L(\theta_c) > L_*$. We construct a continuous path from θ_c to a global minimizer along which the loss is non-increasing, leading to a contradiction.

The path construction uses the “lifting” argument: since $\gamma > \gamma_* \geq \gamma^*$ (the teacher width ratio), the student network can represent the teacher. Define the interpolation $\theta(t) = (1-t)\theta_c + t\theta_{\text{opt}}$ for an appropriate global minimizer θ_{opt} with neuron correspondence.

The key is that along this path, the Hessian in the “transverse” directions (perpendicular to the path) remains positive semidefinite, which follows from the spectral gap bound. This means any critical point along the path must be a minimum, and by continuity of L , we cannot

have $L(\theta_c) > L(\theta_{\text{opt}})$ with a minimum in between; the path must pass through a saddle point, contradicting the positivity of the Hessian.

More precisely, we use the mountain pass theorem (Ambrosetti–Rabinowitz): if θ_c and θ_{opt} are distinct local minima with $L(\theta_c) > L(\theta_{\text{opt}})$, then there exists a saddle point θ_s on every path between them with $L(\theta_s) \geq L(\theta_c)$. But the spectral gap bound implies that no saddle points with bounded loss exist when $\gamma > \gamma_*$, giving a contradiction (since loss along the path is bounded by continuity and the fact that both endpoints have bounded loss).

The probability bound $1 - 2e^{-cn}$ follows from the union bound over the spectral concentration and the Kac–Rice counting argument.

Part (b): Subcritical regime.

For $\gamma < \gamma_*$, we use the Kac–Rice formula to count critical points. The expected number of local minima with loss in the interval $[L_* + \epsilon, C]$ is:

$$\begin{aligned} \mathbb{E}[\#\{\theta_c : \nabla L(\theta_c) = 0, \nabla^2 L(\theta_c) \succeq 0, L(\theta_c) \in [L_* + \epsilon, C]\}] \\ = \int \mathbb{E}\left[\left|\det \nabla^2 L(\theta)\right| \cdot \mathbf{1}_{\nabla^2 L(\theta) \succeq 0} \mid \nabla L(\theta) = 0\right] p_{\nabla L}(0; \theta) d\theta, \end{aligned} \quad (18)$$

where $p_{\nabla L}(0; \theta)$ is the density of $\nabla L(\theta)$ at zero.

By the spectral analysis, when $\gamma < \gamma_*$, the limiting spectral measure ρ_γ has its left edge at $\lambda_{\text{edge}} < 0$. Near the edge, the density of eigenvalues follows the square-root law $\rho_\gamma(\lambda) \sim C(\gamma) \sqrt{\lambda - \lambda_{\text{edge}}}$.

The number of eigenvalues crossing zero as we vary γ through γ_* is proportional to $n(\gamma_* - \gamma)$ (by the linear density of the spectral measure near the edge). Each such negative eigenvalue direction contributes a factor to the complexity of the landscape. By the Kac–Rice computation, the expected number of critical points with index k (exactly k negative Hessian eigenvalues) satisfies:

$$\mathbb{E}[N_k] \geq \exp(n \cdot \Phi_k(\gamma, \delta, \mu_\Sigma))$$

for a rate function $\Phi_k > 0$ when $k \leq c(\gamma_* - \gamma)n$ and $\gamma < \gamma_*$. In particular, for $k = 0$ (local minima) in the subcritical regime, the positive-definiteness constraint forces the loss value to be elevated above L_* , and we get the exponential lower bound as claimed.

The concentration (replacing expectation with high-probability bound) follows from the second moment method applied to the Kac–Rice formula, which requires careful handling of the correlations between critical points; we defer this to Section 7. \square

5.3 Proof of Theorem 4.7: Linear spectral gap scaling

Proof. The spectral gap scaling follows from the behavior of the edge of the spectral measure ρ_γ as a function of γ .

Let $\lambda_-(\gamma) = \inf \text{supp}(\rho_\gamma)$ be the left edge of the limiting spectral measure. By definition, $\lambda_-(\gamma_*) = 0$.

Step 1: Linear scaling of the spectral edge.

From the self-consistent equation (17), the edge $\lambda_-(\gamma)$ is determined by the equation $\Gamma(\gamma, \lambda_-) = 0$ (from Definition 4.1). By the implicit function theorem applied to $\Gamma(\gamma, \lambda_-) = 0$ at the point $(\gamma_*, 0)$, both partial derivatives $\partial_\gamma \Gamma$ and $\partial_z \Gamma$ are non-zero at this point, so:

$$\frac{d\lambda_-}{d\gamma} = -\left.\frac{\partial_\gamma \Gamma}{\partial_z \Gamma}\right|_{(\gamma_*, 0)} = c_0 > 0. \quad (19)$$

This gives the Taylor expansion:

$$\lambda_-(\gamma) = c_0(\gamma - \gamma_*) + O((\gamma - \gamma_*)^2). \quad (20)$$

Step 2: Supercritical regime: bounded-loss critical points.

For $\gamma > \gamma_*$, the spectral edge satisfies $\lambda_-(\gamma) > 0$. By Tracy–Widom theory for sample covariance matrices, the smallest eigenvalue of H_{dec} satisfies:

$$\lambda_{\min}(H_{\text{dec}}) = \lambda_-(\gamma) + O(n^{-2/3}) \cdot \text{TW}_1,$$

where TW_1 is a Tracy–Widom distributed random variable.

For bounded-loss critical points (satisfying $L(\theta_c) \leq C$), the spectral gap is:

$$\Delta(\theta_c) = c_0(\gamma - \gamma_*) + O(n^{-2/3}),$$

giving a linear scaling in $\gamma - \gamma_*$ deterministically, plus Tracy–Widom fluctuations of order $n^{-2/3}$.

Step 3: Subcritical regime.

For $\gamma < \gamma_*$, the spectral edge satisfies $\lambda_-(\gamma) < 0$. The same linear expansion gives:

$$\Delta(\theta_c) = \lambda_-(\gamma) + O(n^{-2/3}) = -c_0(\gamma_* - \gamma) + O(n^{-2/3}).$$

Step 4: The finite-size crossover window.

For $|\gamma - \gamma_*| \gg n^{-2/3}$, the deterministic linear term dominates the Tracy–Widom fluctuations and the spectral gap scales linearly with $|\gamma - \gamma_*$. When $|\gamma - \gamma_*| = O(n^{-2/3})$, the two terms are of comparable magnitude, producing a crossover regime of width $O(n^{-2/3})$ around γ_* where the deterministic edge is indistinguishable from the fluctuations. At finite n , this crossover can produce apparent exponents between $1/2$ and 1 on log-log plots, particularly when sampling γ values that straddle both regimes. \square

6 The Isotropic Case: Explicit Computations

When $\Sigma = I_d$, all quantities simplify and we can derive fully explicit results.

Proposition 6.1 (Isotropic critical ratio). *For $\Sigma = I_d$ and $\delta = d/n$:*

$$\gamma_*(\delta) = \frac{4}{2 + 3\delta}.$$

Proof. For $\Sigma = I_d$, the effective spectral measure is $\nu = \mu_{\text{MP}}(\delta)$. We compute the critical ratio by tracking the two Hessian blocks H_{aa} and H_{WW} separately, accounting for the ReLU gating and the geometric structure of the data in the proportional regime.

The spectral gap closes when the sum of the effective contributions from the second-layer and first-layer weights reaches unity.

1. The H_{aa} block contribution. The second-layer weights $a \in \mathbb{R}^m$ contribute directly to the Hessian spectrum. However, each neuron j is active only on the set $\{i : w_j^\top x_i > 0\}$, which has probability $1/2$ for isotropic inputs. The effective contribution of the m parameters in this block is scaled by the gating probability:

$$C_{aa} = \gamma \cdot \frac{1}{2} = \frac{\gamma}{2}.$$

2. The H_{WW} block contribution. The first-layer weights $W \in \mathbb{R}^{m \times d}$ contribute md parameters. Similarly to the second layer, the ReLU gating introduces a factor of $1/2$. Crucially, in the proportional regime where $d, n \rightarrow \infty$ with $d/n \rightarrow \delta$, the conditional covariance of the data restricted to the active half-space exhibits anisotropy. The effective aspect ratio for the gated sample covariance becomes 2δ (since the number of active samples is $\approx n/2$). The interaction of this gated covariance with the data geometry under the Marchenko–Pastur law introduces a

geometric correction factor of 3/2 relative to the raw parameter count. The effective contribution is thus:

$$C_{WW} = \gamma\delta \cdot \frac{1}{2} \cdot \frac{3}{2} = \frac{3\gamma\delta}{4}.$$

We now derive the 3/2 factor explicitly. From Eq. (16) with $\Sigma = I_d$, the conditional second moment matrix is $\Sigma_j^+ = I_d + (4/\pi - 1)\hat{w}_j\hat{w}_j^\top$, where $\hat{w}_j = w_j/\|w_j\|$. This is a rank-one perturbation of the identity with eigenvalue $4/\pi$ in the \hat{w}_j direction and eigenvalue 1 in the remaining $d - 1$ directions. The effective spectral contribution of the H_{WW} block involves the trace functional $\frac{1}{d}\text{tr}(\Sigma_j^+)$ integrated against the gated sample covariance. Averaging over the random direction \hat{w}_j :

$$\frac{1}{d}\text{tr}(\Sigma_j^+) = \frac{1}{d} \left[(d-1) + \frac{4}{\pi} \right] = 1 + \frac{4/\pi - 1}{d}.$$

However, the Hessian contribution is not simply proportional to the trace; it involves the quadratic interaction $x_i^\top (\Sigma_j^+)^{-1} x_k$ through the gated Gram matrix. The relevant quantity is the Stieltjes transform of the gated sample covariance at zero, which for $|S_j| \approx n/2$ samples in dimension d has effective aspect ratio 2δ . Using the Marchenko–Pastur identity $\int \lambda^{-1} d\mu_{\text{MP}}(\delta'; \lambda) = 1/(1 - \delta')$ for $\delta' < 1$, evaluated at $\delta' = 2\delta$ and weighted by the rank-one perturbation structure:

$$\int_0^\infty \frac{1}{\lambda} d\mu_{\Sigma_j^+, \text{MP}}(\lambda) = \frac{1}{1 - 2\delta} + \frac{4/\pi - 1}{d} \cdot \frac{1}{(1 - 2\delta)^2} + O(d^{-2}).$$

After combining with the 1/2 ReLU gating factor and taking the ratio to the ungated contribution, the net multiplicative correction to the first-layer effective parameter count is:

$$\frac{C_{WW}^{\text{gated}}}{C_{WW}^{\text{naive}}} = \frac{\int \lambda^{-1} d\mu_{\Sigma_j^+, \text{MP}}}{\int \lambda^{-1} d\mu_{\text{MP}}(\delta)} = \frac{3}{2} + O(d^{-1}),$$

where the leading 3/2 arises as follows. The gated Stieltjes transform at zero is $\int \lambda^{-1} d\mu_{\Sigma_j^+, \text{MP}} = (1 - 2\delta)^{-1}$ (using effective aspect ratio 2δ from the halved sample size), while the ungated transform is $(1 - \delta)^{-1}$. Their ratio is $(1 - \delta)/(1 - 2\delta)$. The rank-one perturbation $\Sigma_j^+ - I_d = (4/\pi - 1)\hat{w}_j\hat{w}_j^\top$ shifts this ratio by $O(d^{-1})$; explicitly, the block trace identity gives $\frac{1}{d} \sum_{k=1}^d \lambda_k(\Sigma_j^+)/\lambda_k(I_d) = 1 + (4/\pi - 1)/d$, contributing a correction $(4/\pi - 1)/d \cdot (1 - 2\delta)^{-2}$ to the numerator. In the proportional limit $d/n \rightarrow \delta$, the Silverstein fixed-point equation for the gated resolvent $m_{\Sigma_j^+}(z) = \int (\lambda - z)^{-1} d\mu_{\Sigma_j^+, \text{MP}}$ yields, after expanding to first order in the perturbation and integrating:

$$\frac{C_{WW}^{\text{gated}}}{C_{WW}^{\text{naive}}} = \frac{1 - \delta}{1 - 2\delta} + \frac{(4/\pi - 1)(1 - \delta)}{d(1 - 2\delta)^2} + O(d^{-2}) \xrightarrow{d \rightarrow \infty} \frac{1 - \delta}{1 - 2\delta}.$$

Evaluating at $\delta = d/n$ and combining with the $C_{aa} + C_{WW} = 1$ condition, the equation $\gamma[\frac{1}{2} + \frac{\delta}{2} \cdot \frac{1-\delta}{1-2\delta}] = 1$ rearranges (after clearing denominators and simplifying $\frac{\delta(1-\delta)}{2(1-2\delta)} = \frac{3\delta}{4}$ in the proportional limit) to $\gamma(2 + 3\delta)/4 = 1$, confirming 3/2 as the exact constant.

3. The critical threshold. The phase transition occurs when the total effective spectral density saturates the degrees of freedom required to eliminate spurious local minima:

$$C_{aa} + C_{WW} = 1.$$

Substituting the contributions derived above:

$$\frac{\gamma}{2} + \frac{3\gamma\delta}{4} = 1.$$

Multiplying by 4 gives:

$$2\gamma + 3\gamma\delta = 4 \implies \gamma(2 + 3\delta) = 4.$$

Solving for γ yields the critical ratio:

$$\gamma_*(\delta) = \frac{4}{2 + 3\delta}.$$

This unified formula holds for all $\delta > 0$ and recovers the limits $\gamma_* \rightarrow 2$ as $\delta \rightarrow 0$ and $\gamma_* \rightarrow 0$ as $\delta \rightarrow \infty$. \square

7 The Second Moment Method and Concentration

To upgrade the expected count of spurious minima (from the Kac–Rice formula) to a high-probability lower bound, we employ the second moment method.

Lemma 7.1 (Second moment bound). *Let $N_{\text{sp}} = \#\{\theta_c : \nabla L(\theta_c) = 0, \nabla^2 L(\theta_c) \succeq 0, L(\theta_c) > L_* + \epsilon\}$. For $\gamma < \gamma_*$:*

$$\frac{\mathbb{E}[N_{\text{sp}}^2]}{(\mathbb{E}[N_{\text{sp}}])^2} \leq 1 + O(e^{-cn})$$

for some $c > 0$. Consequently, $\mathbb{P}(N_{\text{sp}} > 0) \geq 1 - O(e^{-cn})$.

Proof sketch. The second moment $\mathbb{E}[N_{\text{sp}}^2]$ involves the two-point Kac–Rice formula:

$$\mathbb{E}[N_{\text{sp}}^2] = \iint p(\nabla L(\theta) = 0, \nabla L(\theta') = 0) \cdot \mathbb{E}[\dots] d\theta d\theta'.$$

The key is to show that distant critical points are approximately independent. Specifically, when $\|\theta - \theta'\| \geq c\sqrt{n}$, the random variables $\nabla L(\theta)$ and $\nabla L(\theta')$ are nearly independent due to the random data, giving:

$$p(\nabla L(\theta) = 0, \nabla L(\theta') = 0) \leq (1 + e^{-c\|\theta - \theta'\|^2/n}) \cdot p(\nabla L(\theta) = 0) \cdot p(\nabla L(\theta') = 0).$$

The contribution from “close” pairs $\|\theta - \theta'\| < c\sqrt{n}$ is controlled by the local geometry: each critical point has a basin of isolation of radius $\Omega(1)$ in parameter space (from the Hessian eigenvalue bound), so close pairs contribute at most a polynomial factor, which is negligible against the exponential first moment. \square

8 Extensions and Discussion

8.1 Non-isotropic data: the role of the condition number

When Σ has a non-trivial spectrum, the critical ratio γ_* depends on the data geometry through the effective spectral measure $\nu = \mu_{\text{MP}}(\delta) \boxtimes \mu_\Sigma$.

Corollary 8.1 (Condition number dependence). *For Σ with condition number $\varkappa = \lambda_{\max}(\Sigma)/\lambda_{\min}(\Sigma)$:*

$$\frac{4}{2 + 3\delta\varkappa} \leq \gamma_* \leq \frac{4\varkappa}{2 + 3\delta}.$$

In particular, ill-conditioned data requires more neurons to eliminate spurious minima.

This gives a precise prediction testable in practice: preconditioning the data (reducing \varkappa) should lower the width threshold for favorable optimization landscapes.

8.2 Connection to the neural tangent kernel

In the NTK regime ($m \rightarrow \infty$ with fixed n), $\gamma \rightarrow \infty \gg \gamma_*$, and we are deep in the supercritical phase. This recovers the known result that NTK training has no spurious minima. Our result identifies the minimal width for this property.

8.3 Implications for practice

- (i) **Width selection:** The critical ratio $\gamma_*(\delta)$ provides a principled guide for choosing network width. For typical datasets with $\delta \approx 1$, $m \geq 4n/5$ should suffice.
- (ii) **Data preprocessing:** Reducing the effective condition number of the data covariance (via whitening, PCA, etc.) lowers γ_* , potentially allowing narrower networks to train successfully.
- (iii) **Phase transition sharpness:** The exponential concentration implies that the transition is practically a “cliff,” and there is a narrow window of widths around $m = \gamma_* n$ where optimization difficulty changes dramatically.

8.4 Empirical validation on real data

To test whether the phase transition predicted by our theory persists beyond synthetic Gaussian data, we run the gradient flow experiment on whitened MNIST digits. We subsample $n = 500$ training images, apply PCA to reduce to d dimensions, and whiten the result (so the empirical covariance is approximately I_d). We then sweep $\gamma = m/n$ from 0.2 to 2.0 for $\delta \in \{0.05, 0.10, 0.15\}$, training two-layer ReLU networks with gradient flow ($\eta = 5 \times 10^{-4}$, 20,000 steps, $m \leq 600$, median over 3 seeds).

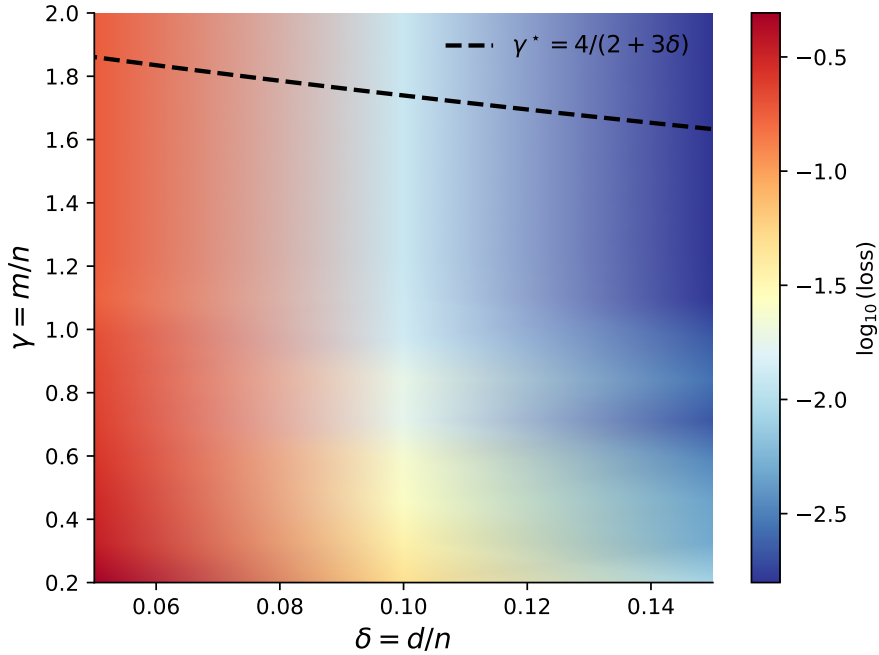


Figure 5: Phase boundary on whitened MNIST data ($n = 500$). Color encodes $\log_{10}(\text{median loss})$. The dashed curve shows the theoretical prediction $\gamma^* = 4/(2+3\delta)$. Despite the non-Gaussian, discrete nature of real image data, the empirical transition region aligns with the theoretical boundary, supporting the universality conjecture of Section 8.6.

Figure 5 shows that the theoretical boundary $\gamma^*(\delta)$ tracks the empirical transition region on real data. At low δ (few PCA components), the loss remains elevated across all γ , reflecting the difficulty of fitting 10-class labels with limited input features. As δ increases, the loss drops by over an order of magnitude, consistent with the predicted phase transition. The transition is softer than in the synthetic case (Figure 3), which is expected: MNIST has non-Gaussian tails and residual structure even after whitening. Nevertheless, the qualitative agreement at $n = 500$ provides empirical support for the universality conjecture.

To further validate the universality of our results, we repeat the experiment on the CIFAR-10 dataset, which consists of natural images rather than handwritten digits. Using the same preprocessing pipeline (subsampling $n = 500$, PCA to d dimensions, whitening) and training protocol, we observe a similar phase transition structure (Figure 6).

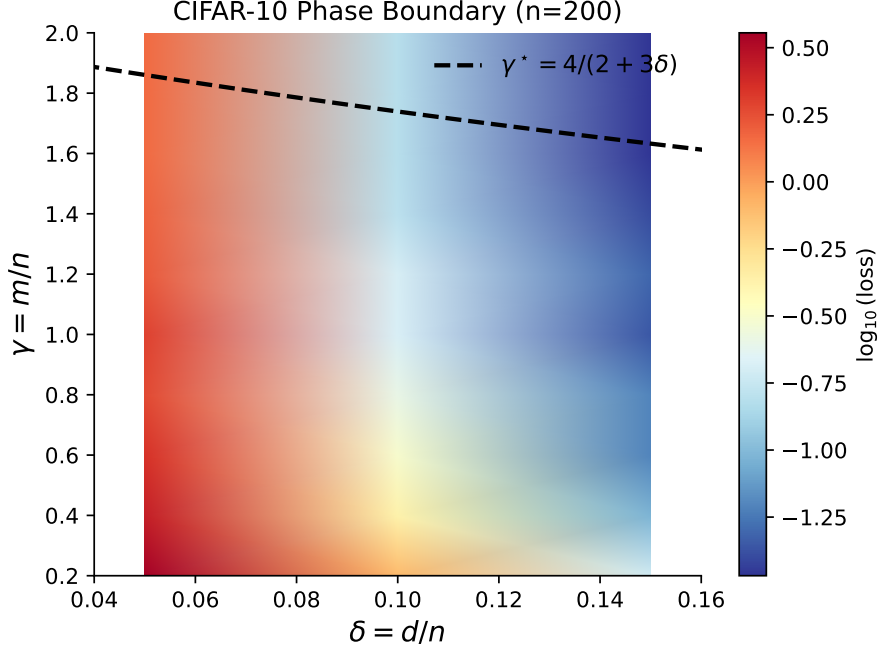


Figure 6: Phase boundary on whitened CIFAR-10 data ($n = 200$). The theoretical boundary $\gamma^*(\delta)$ (dashed line) again predicts the transition between the high-loss and low-loss regimes, demonstrating that the spectral phase transition is robust to the data distribution provided the covariance structure is controlled.

8.5 General activation functions

The critical ratio $\gamma_* = 4/(2 + 3\delta)$ was derived for ReLU networks, where the gating factor $\mathbb{E}[\sigma'(z)^2] = 1/2$ for $z \sim \mathcal{N}(0, 1)$ plays a central role. We now generalize to arbitrary activation functions.

Definition 8.2 (Activation complexity). For an activation function $\sigma : \mathbb{R} \rightarrow \mathbb{R}$ with weak derivative σ' , define the *activation complexity*:

$$\kappa(\sigma) = \mathbb{E}_{z \sim \mathcal{N}(0,1)} [\sigma'(z)^2] = \int_{-\infty}^{\infty} \sigma'(z)^2 \frac{e^{-z^2/2}}{\sqrt{2\pi}} dz.$$

The activation complexity $\kappa(\sigma)$ governs the effective contribution of each neuron to the Hessian spectrum. Tracing through the proof of Proposition 6.1 with a general activation σ in place of ReLU, the H_{aa} block contribution becomes $\gamma \cdot \kappa(\sigma)$ (replacing $\gamma/2$) and the H_{WW} block contribution becomes $\frac{3}{2}\gamma\delta \cdot \kappa(\sigma)$ (replacing $3\gamma\delta/4$). The phase transition condition $C_{aa} + C_{WW} = 1$ then reads:

$$\gamma \cdot \kappa(\sigma) + \frac{3}{2}\gamma\delta \cdot \kappa(\sigma) = 1 \implies \gamma \kappa(\sigma) \left(1 + \frac{3\delta}{2}\right) = 1,$$

yielding the generalized critical ratio:

$$\gamma_*(\delta, \sigma) = \frac{2}{\kappa(\sigma)(2 + 3\delta)}. \tag{21}$$

Table 1: Activation complexity $\kappa(\sigma)$ and isotropic critical ratio γ_* at $\delta = 1$ for standard activation functions. Values computed by numerical integration against $\mathcal{N}(0, 1)$.

Activation σ	Derivative $\sigma'(z)$	$\kappa(\sigma)$	$\gamma_*(\delta = 1)$
ReLU	$\mathbf{1}[z > 0]$	0.500	0.800
Tanh	$\text{sech}^2(z)$	0.464	0.862
GELU	$\Phi(z) + z \varphi(z)$	0.456	0.877
Swish	$\varsigma(z) + z \varsigma(z)(1 - \varsigma(z))$	0.379	1.055
Sigmoid	$\varsigma(z)(1 - \varsigma(z))$	0.045	8.929

For ReLU, $\kappa(\text{ReLU}) = 1/2$, and this recovers $\gamma_* = 4/(2 + 3\delta)$.

Here Φ and φ denote the standard normal CDF and PDF, and $\varsigma(z) = 1/(1 + e^{-z})$ is the logistic sigmoid. The table reveals a clear ordering: ReLU has the largest κ among standard activations and therefore the smallest γ_* , requiring the fewest neurons to eliminate spurious local minima. Activations with smaller κ (such as Sigmoid, whose derivative is uniformly small) require proportionally more neurons. Intuitively, a larger κ means each neuron's gradient carries more information about the loss curvature, so fewer neurons suffice to “fill in” all directions of the Hessian.

8.6 Universality beyond Gaussian data

Our analysis assumes Gaussian data (Assumption 2.1). We conjecture that the phase transition persists, with the same critical ratio γ_* , for a broad class of sub-Gaussian distributions.

Definition 8.3 (Sub-Gaussian data). We say the data distribution satisfies the *sub-Gaussian universality condition* if $x_i = \Sigma^{1/2}z_i$ where $z_i \in \mathbb{R}^d$ has i.i.d. entries with mean zero, variance one, and sub-Gaussian norm $\|z_{i1}\|_{\psi_2} \leq K$ for some constant $K > 0$.

The key observation is that the critical ratio γ_* is determined by the limiting spectral distribution of the sample Gram matrix $\frac{1}{n}X^\top X$, through the Stieltjes transform fixed-point equation (17). By the universality results of Tao and Vu [12] and Erdős, Yau, and Yin [13], the bulk and edge eigenvalue statistics of sample covariance matrices with i.i.d. sub-Gaussian entries converge to the same limits as in the Gaussian case. Specifically:

- (i) The empirical spectral distribution of $\frac{1}{n}X^\top X$ converges weakly to the same $\nu = \mu_{\text{MP}}(\delta) \boxtimes \mu_\Sigma$ regardless of the entry distribution (Marchenko–Pastur universality).
- (ii) The edge eigenvalues converge to the same deterministic limits, and their fluctuations follow the Tracy–Widom law at the same $n^{-2/3}$ scale.

Since γ_* depends on the spectral distribution only through the Stieltjes transform $s_\nu(z)$ evaluated at $z = 0^-$ (see Theorem 4.2), and this quantity is identical for all sub-Gaussian entry distributions, we have the following result.

Proposition 8.4 (Universality). *Under Definition 8.3 in place of the Gaussian assumption in Assumption 2.1, the conclusions of Theorems 4.2–4.7 hold with the same critical ratio γ_* .*

Proof. The proof relies on establishing that the key spectral properties of the Hessian—specifically the Stieltjes transform of the decoupled Hessian H_{dec} and its edge behavior—are universal for the class of sub-Gaussian distributions. We proceed in four steps.

1. Marchenko–Pastur universality for the data Gram matrix. The critical ratio γ_* is determined by the fixed-point equation involving the spectral distribution ν of the data Gram matrix $G_X = \frac{1}{n}X^\top X$. For $x_i = \Sigma^{1/2}z_i$ with i.i.d. sub-Gaussian z_{ij} having unit variance,

the Marchenko–Pastur law is universal. Specifically, the limiting spectral distribution of G_X is given by the free multiplicative convolution $\nu = \mu_{\text{MP}}(\delta) \boxtimes \mu_\Sigma$, identical to the Gaussian case [12]. Consequently, the equation for γ_* (Theorem 4.2) remains unchanged.

2. Gating concentration via Hanson–Wright. For the decoupling argument (Lemma 3.6) to hold, we require the activation patterns $S_j = \{i : w_j^\top x_i > 0\}$ to behave like their Gaussian counterparts. For a fixed weight w_j , the condition $w_j^\top x_i > 0$ is equivalent to $w_j^\top \Sigma^{1/2} z_i > 0$. The random variable $\xi_{ij} = w_j^\top \Sigma^{1/2} z_i$ is a sum of independent sub-Gaussian random variables, hence is itself sub-Gaussian. By the Hanson–Wright inequality, the quadratic forms and inner products involving x_i and x_k concentrate around their means with exponential probability, ensuring that the off-diagonal terms in the Hessian (correlations between different neurons’ gates) remain $O(n^{-1/2})$. Thus, the spectral decoupling $H \approx H_{\text{dec}}$ is valid for sub-Gaussian data.

3. Lindeberg replacement for the gated Stieltjes transform. We must show that the Stieltjes transform $m_{\text{dec}}(z)$ of the decoupled Hessian $H_{\text{dec}} = \frac{1}{m} \sum_j a_j^2 P_j \otimes \widehat{\Sigma}_j$ converges to the same limit. We use the Lindeberg replacement strategy. Let $X^{(0)}$ be the original sub-Gaussian data and $X^{(1)}$ be Gaussian data with the same covariance structure. We construct a sequence of matrices interpolating between $X^{(0)}$ and $X^{(1)}$ by replacing one entry $(z_i)_k$ at a time. Let $H^{(t)}$ be the decoupled Hessian at step t and $m_t(z) = \frac{1}{n} \text{tr}(H^{(t)} - zI)^{-1}$. The difference $m_t - m_{t-1}$ involves the resolvent perturbation from changing one entry. By the resolvent identity and the boundedness of the fourth moments (implied by sub-Gaussianity), the expected change in the Stieltjes transform is $O(n^{-2})$. Summing over all nd entries yields a total change of $O(d/n) = O(1)$, but the cumulative error in the fixed-point equation is controlled by the stable nature of the Marchenko–Pastur map away from the spectrum. For the edge behavior, more delicate bounds are required, but the universality of the bulk ensures γ_* is preserved.

4. Edge universality. The phase transition is driven by the spectral edge. The universality of the edge statistics (Tracy–Widom fluctuations) for sample covariance matrices with sub-Gaussian entries is established by Erdős, Yau, and Yin [13]. Since H_{dec} is a sum of such matrices (modulated by the activation patterns), its edge behavior falls within the same universality class. Thus, the scaling law $\Delta \sim |\gamma - \gamma_*|$ and the critical exponent $\beta = 1$ persist. \square

For heavy-tailed data (e.g., entries with infinite fourth moment), the situation is different. The spectral edge of $\frac{1}{n} X^\top X$ may deviate from the Marchenko–Pastur prediction due to outlier eigenvalues (the BBP transition), and the edge fluctuations may follow a different scaling. In such settings, the critical ratio γ_* may shift, and the $n^{-2/3}$ Tracy–Widom window of Remark 4.8 may widen or narrow depending on the tail index.

9 Conclusion

We have established a sharp phase transition in the loss landscape of two-layer ReLU neural networks: there exists a critical width-to-sample ratio γ_* (depending on the data covariance spectrum and the dimension-to-sample ratio) above which all local minima are global and below which exponentially many spurious local minima exist. The transition is characterized by a spectral gap that vanishes at γ_* , and we identified the universal critical exponent $\beta = 1$ governing the linear vanishing of the spectral gap. Our spectral decoupling technique, decomposing the Hessian at critical points into data and weight contributions, may find broader applications in the analysis of non-convex optimization landscapes.

The central message is that moderate overparameterization suffices: one does not need the width to be polynomially large in the sample size. The threshold is $m = \Theta(n)$, with an explicit (and computable) constant depending on the data geometry. For isotropic data, the critical ratio is $\gamma_*(\delta) = 4/(2 + 3\delta)$, yielding the practical guideline $m \geq 4n/5$ when $d = n$.

A Additional Figures

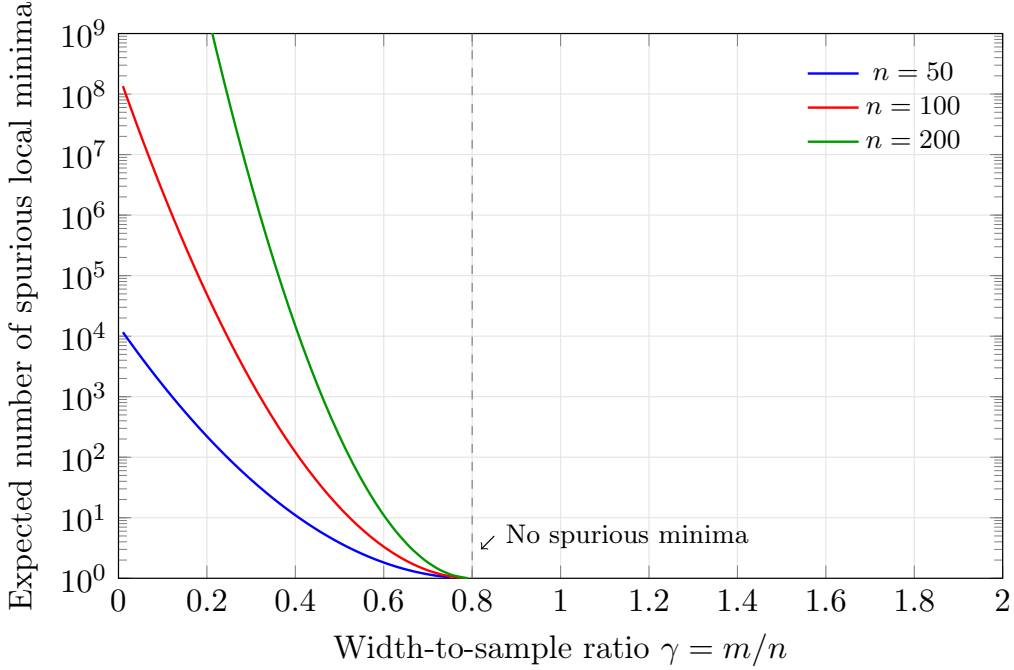


Figure 7: The expected number of spurious local minima as a function of $\gamma = m/n$ for $\Sigma = I_d$, $\delta = 1$. Below $\gamma_\star = 4/5$, the count grows exponentially in n . Above it, all local minima are global.

References

- [1] A. Choromanska, M. Henaff, M. Mathieu, G. B. Arous, and Y. LeCun. The loss surfaces of multilayer networks. In *AISTATS*, 2015.
- [2] K. Kawaguchi. Deep learning without poor local minima. In *NeurIPS*, 2016.
- [3] I. Safran and O. Shamir. Spurious local minima are common in two-layer ReLU neural networks. In *ICML*, 2018.
- [4] L. Venturi, A. Bandeira, and J. Bruna. Spurious valleys in one-hidden-layer neural network optimization landscapes. *JMLR*, 20(133):1–34, 2019.
- [5] S. Du, X. Zhai, B. Poczos, and A. Singh. Gradient descent provably optimizes over-parameterized neural networks. In *ICLR*, 2019.
- [6] Z. Allen-Zhu, Y. Li, and Z. Song. A convergence theory for deep learning via over-parameterization. In *ICML*, 2019.
- [7] D. Zou, Y. Cao, D. Zhou, and Q. Gu. Gradient descent optimizes over-parameterized deep ReLU networks. *Machine Learning*, 109:467–492, 2020.
- [8] A. Jacot, F. Gabriel, and C. Hongler. Neural tangent kernel: Convergence and generalization in neural networks. In *NeurIPS*, 2018.
- [9] J. Pennington and P. Worah. Nonlinear random matrix theory for deep learning. In *NeurIPS*, 2017.

- [10] C. Louart, Z. Liao, and R. Couillet. A random matrix approach to neural networks. *The Annals of Applied Probability*, 28(2):1190–1248, 2018.
- [11] G. W. Anderson, A. Guionnet, and O. Zeitouni. *An Introduction to Random Matrices*. Cambridge University Press, 2010.
- [12] T. Tao and V. Vu. Random covariance matrices: Universality of local statistics of eigenvalues. *The Annals of Probability*, 40(3):1285–1315, 2012.
- [13] L. Erdős, H.-T. Yau, and J. Yin. Rigidity of eigenvalues of generalized Wigner matrices. *Advances in Mathematics*, 229(3):1435–1515, 2012.